



A Lumped Two-Compartment Model for Simulation of Ventricular Pump and Tissue Mechanics in Ischemic Heart Disease

Tijmen Koopsen^{1*}, Nick Van Osta¹, Tim Van Loon¹, Frans A. Van Nieuwenhoven², Frits W. Prinzen², Bas R. Van Klarenbosch³, Feddo P. Kirkels³, Arco J. Teske³, Kevin Vernooij^{4,5}, Tammo Delhaas¹ and Joost Lumens¹

¹Department of Biomedical Engineering, Cardiovascular Research Institute Maastricht (CARIM), Maastricht University, Maastricht, Netherlands, ²Department of Physiology, Cardiovascular Research Institute Maastricht (CARIM), Maastricht University, Maastricht, Netherlands, ³Division of Heart and Lungs, Department of Cardiology, University Medical Center Utrecht, Utrecht, Netherlands, ⁴Department of Cardiology, Cardiovascular Research Institute Maastricht (CARIM), Maastricht University Medical Center, Maastricht, Netherlands, ⁵Department of Cardiology, Radboud University Medical Center, Nijmegen, Netherlands

OPEN ACCESS

Edited by:

Alexander Y. Mitrophanov,
National Cancer Institute at Frederick
(NIH), United States

Reviewed by:

Vicky Y. Wang,
The University of Auckland,
New Zealand
Per Lav Madsen,
University of Copenhagen, Denmark

*Correspondence:

Tijmen Koopsen
t.koopsen@maastrichtuniversity.nl

Specialty section:

This article was submitted to
Computational Physiology and
Medicine,
a section of the journal
Frontiers in Physiology

Received: 24 September 2021

Accepted: 10 March 2022

Published: 11 May 2022

Citation:

Koopsen T, Van Osta N, Van Loon T,
Van Nieuwenhoven FA, Prinzen FW,
Van Klarenbosch BR, Kirkels FP,
Teske AJ, Vernooij K, Delhaas T and
Lumens J (2022) A Lumped Two-
Compartment Model for Simulation of
Ventricular Pump and Tissue
Mechanics in Ischemic Heart Disease.
Front. Physiol. 13:782592.
doi: 10.3389/fphys.2022.782592

Introduction: Computational modeling of cardiac mechanics and hemodynamics in ischemic heart disease (IHD) is important for a better understanding of the complex relations between ischemia-induced heterogeneity of myocardial tissue properties, regional tissue mechanics, and hemodynamic pump function. We validated and applied a lumped two-compartment modeling approach for IHD integrated into the CircAdapt model of the human heart and circulation.

Methods: Ischemic contractile dysfunction was simulated by subdividing a left ventricular (LV) wall segment into a hypothetical contractile and noncontractile compartment, and dysfunction severity was determined by the noncontractile volume fraction (*NCVF*). Myocardial stiffness was determined by the zero-passive stress length ($L_{s0,pas}$) and nonlinearity (k_{ECM}) of the passive stress-sarcomere length relation of the noncontractile compartment. Simulated end-systolic pressure volume relations (ESPVRs) for 20% acute ischemia were qualitatively compared between a two- and one-compartment simulation, and parameters of the two-compartment model were tuned to previously published canine data of regional myocardial deformation during acute and prolonged ischemia and reperfusion. In six patients with myocardial infarction (MI), the *NCVF* was automatically estimated using the echocardiographic LV strain and volume measurements obtained acutely and 6 months after MI. Estimated segmental *NCVF* values at the baseline and 6-month follow-up were compared with percentage late gadolinium enhancement (LGE) at 6-month follow-up.

Results: Simulation of 20% of *NCVF* shifted the ESPVR rightward while moderately reducing the slope, while a one-compartment simulation caused a leftward shift with severe reduction in the slope. Through tuning of the *NCVF*, $L_{s0,pas}$, and k_{ECM} , it was found that manipulation of the *NCVF* alone reproduced the deformation during acute ischemia and reperfusion, while additional manipulations of $L_{s0,pas}$ and k_{ECM} were required to

reproduce deformation during prolonged ischemia and reperfusion. Out of all segments with LGE>25% at the follow-up, the majority (68%) had higher estimated *NCVF* at the baseline than at the follow-up. Furthermore, the baseline *NCVF* correlated better with percentage LGE than *NCVF* did at the follow-up.

Conclusion: We successfully used a two-compartment model for simulation of the ventricular pump and tissue mechanics in IHD. Patient-specific optimizations using regional myocardial deformation estimated the *NCVF* in a small cohort of MI patients in the acute and chronic phase after MI, while estimated *NCVF* values closely approximated the extent of the myocardial scar at the follow-up. In future studies, this approach can facilitate deformation imaging-based estimation of myocardial tissue properties in patients with cardiovascular diseases.

Keywords: myocardial infarction, computational modeling and simulation, deformation imaging, contractile dysfunction, strain

1 INTRODUCTION

Computational modeling of cardiac mechanics and hemodynamics in ischemic heart disease (IHD) is important for better understanding of the complex relations between ischemia-induced heterogeneity of myocardial tissue properties, regional tissue mechanics, and hemodynamic pump function. Spatially detailed three-dimensional models based on the finite element method (FEM) are most frequently used for simulation of myocardial infarction (MI) and its effects on cardiac geometry, tissue mechanics, and electrophysiology. While many studies have successfully used FEM models for investigating the pathophysiology and potential treatment of MI (Fomovsky et al., 2011; Fomovsky et al., 2012; Rouillard and Holmes, 2014; Veress et al., 2015; Leong et al., 2017; Haddad and Samani, 2018; Wang et al., 2018; Chan et al., 2019; Fan et al., 2019; Zhuan et al., 2019; Estrada et al., 2020; Zhang et al., 2020; Zhang et al., 2021), complexity of these models can provide a problem when performing simulations on a patient-specific level (Moulton et al., 2017).

Reduced-order modeling approaches with sufficient spatial and physiological details to accurately simulate global and regional tissue mechanics are important for patient-specific simulation of MI (Moulton et al., 2017; Holmes and Lumens, 2018). The CircAdapt lumped-parameter model of the human heart and circulation is a closed-loop model which simulates real-time, beat-to-beat hemodynamics and mechanics of the heart and blood vessels (Arts et al., 2004; Lumens et al., 2009). Previous studies using CircAdapt have shown that the model realistically simulates global ventricular hemodynamics and regional myocardial mechanics in various pathological conditions (Lumens et al., 2009; Walmsley et al., 2015). However, its ability to simulate the effects of ischemia-induced contractile dysfunction on both global pump and regional tissue mechanics has not been evaluated yet.

In this study, we presented and tested a modeling approach for MI-induced myocardial contractile dysfunction, which is integrated into the CircAdapt modeling framework. Following previous observations by Sunagawa et al. (1982), who showed that

global ventricular mechanics during acute regional ischemia were best described using a two-compartment modeling approach, we subdivided an ischemic wall segment into an active and a passive compartment. We validated this two-compartment implementation by comparing its simulated effects of regional ischemia on the global LV pump function against the results of a one-compartment implementation and by tuning parameters of the two-compartment model to mimic existing data on regional myocardial deformation in dogs with coronary artery ligation. We then evaluated whether the model could be used to estimate the severity of regional contractile dysfunction in MI patients by applying an automatic optimization algorithm to measurements of regional myocardial deformation performed within 72 h and after 6 months following MI and by comparing estimated severities to percentage late gadolinium enhancement (LGE) after 6 months.

2 MATERIALS AND METHODS

A brief description of the CircAdapt model components, which are most relevant for this study, are provided as follows. For further details on the CircAdapt model, we referred to previously published validation studies (Walmsley et al., 2015; Lumens et al., 2009). Thereafter, the one- and two-compartment models for ischemia-induced contractile dysfunction were described, and we explained how simulated global mechanics were compared between both modeling approaches. Then, we described how model simulations using the two-compartment model were tuned using existing experimental measurements. Finally, we introduced the clinical data and computational methods used for imaging-based estimation of regional contractile dysfunction in patient hearts acutely and 6 months after MI.

2.1 CircAdapt Model

The CircAdapt computational model of the human heart and circulation is a closed-loop lumped-parameter model that simulates beat-to-beat hemodynamics and mechanics of the heart and blood vessels (Arts et al., 2004; Lumens et al., 2009). The model

uses a simplified ventricular geometry, where cardiac walls are represented by thick-walled spherical shells consisting of myofibers. The TriSeg module allows for interventricular interaction by coupling the left (LV) and right ventricular (RV) walls through the interventricular septum (Lumens et al., 2009). Walls can be subdivided into patches using the MultiPatch module (Walmsley et al., 2015), which enables heterogeneity of myocardial tissue properties within the walls. Myofiber active and passive stress generation is modeled using a three-element Hill model (Arts et al., 2003). In brief, the series contractile element with the time-dependent length $L_{si}(t)$ generates an active stress $\sigma_{f,act}(t)$ which represents the force developed through cross-bridge formation between actin and myosin filaments. The zero-active stress contractile element length $L_{si0,act}$ defines the length at which no active stress is developed. The series elastic element with the time-dependent length $L_{se}(t)$ describes the intrinsic elasticity of the sarcomere, and a reference length of $L_{se,iso}$ is used to define the length of the series elastic element at the onset of isovolumetric contraction. Furthermore, the density of cross-bridge formation is described by a time-dependent contractility state variable $C(t, L_{si}(t))$, while active stress generation is scaled by a parameter $S_{f,act}$. Taken together, active stress is calculated as follows:

$$\sigma_{f,act}(t) = S_{f,act} \cdot C(t, L_{si}(t)) \cdot (L_{si}(t) - L_{si0,act}) \cdot \frac{L_{se}(t)}{L_{se,iso}} \quad (1)$$

Passive myocardial tissue behavior is described by the parallel elastic element, which captures both extracellular and intracellular structures. Therefore, total passive stress $\sigma_{f,pas}(t)$ is the sum of the extracellular matrix stress $\sigma_{f,ECM}(t)$ and intracellular stress, that is, titin stress $\sigma_{f,tit}(t)$:

$$\sigma_{f,pas}(t) = \sigma_{f,ECM}(t) + \sigma_{f,tit}(t) \quad (2)$$

The extracellular matrix stress $\sigma_{f,ECM}(t)$ depends as follows on the total time-dependent sarcomere length $L_s(t)$, which is the sum of $L_{si}(t)$ and $L_{se}(t)$:

$$\sigma_{f,ECM}(t) = S_{f,pas} \cdot \left(\left(\frac{L_s(t)}{L_{s0,pas}} \right)^{k_{ECM}} - 1 \right) \quad (3)$$

Here, $S_{f,pas}$ is a parameter scaling passive stress development, while $L_{s0,pas}$ is the zero-passive stress sarcomere length. The parameter k_{ECM} determines the nonlinearity of the relation. The titin stress $\sigma_{f,tit}(t)$ depends on $L_s(t)$, $S_{f,act}$, $L_{s0,pas}$, and two parameters which scale the development of titin stress ($k_{1,tit}$) and the nonlinearity of the relation ($k_{2,tit}$):

$$\sigma_{f,tit}(t) = S_{f,act} \cdot k_{1,tit} \cdot \left(\left(\frac{L_s(t)}{L_{s0,pas}} \right)^{k_{2,tit}} - 1 \right) \quad (4)$$

2.2 Simulating Ischemia-Induced Contractile Dysfunction: One-Compartment Vs. Two-Compartment Model

In a combined experimental and modeling study, Sunagawa et al. (1982) showed that the LV systolic function during

regional ischemia was best captured by a two-compartment model including an active and a passive compartment. The rationale behind this two-compartment model is that the active compartment lumps all of the normally functioning tissues within the nonischemic and ischemic region, while the passive compartment lumps all of the nonfunctional parts of the ischemic region. As mentioned before, we hypothesized that we could use a similar modeling approach not only for simulating global LV pump mechanics during regional ischemia but also to simulate average regional LV tissue mechanics (i.e., the myofiber stress and strain) in ischemic myocardial segments, which are defined by deformation imaging techniques, for example, speckle tracking echocardiography (STE). In the CircAdapt model, tissue properties are defined per myocardial patch, and by default, each myocardial wall includes one myocardial patch. The active and passive stress of a patch is calculated using Eqs 1–4. To simulate reduced patch contractility, one approach is to reduce parameter $S_{f,act}$ (Eq. 1). Since this approach does not involve subdivision of the myocardial patch into multiple patches (i.e., compartments), we term this as a one-compartment modeling approach for simulating contractile dysfunction. For the two-compartment model of ischemia, the CircAdapt MultiPatch module (Walmsley et al., 2015) is applied. The MultiPatch module has previously been used to subdivide myocardial walls into different patches, each having their own unique tissue properties (Walmsley et al., 2015; Lumens et al., 2015; Voigt et al., 2015). In this study, we applied the MultiPatch module to further subdivide an ischemic myocardial patch with volume V_{patch} into a contractile and a noncontractile patch (i.e., compartment) with volumes V_C and V_{NC} , respectively (Figure 1). Compared to the implementation of Sunagawa et al. (1982), where the subdivided volume V_{patch} equaled the volume of the entire LV wall, we additionally applied the two-compartment model on a regional level, where V_{patch} equals the volume of an echocardiographic segment by approximation. Mechanics of V_C are described by Eqs 1–4, while for V_{NC} it holds $S_{f,act} = 0$; therefore, the mechanics of V_{NC} are fully described by Eq. 3. The degree of patch contractile dysfunction is determined by the noncontractile volume fraction (NCVF), defined as the relative volume of the noncontractile compartment:

$$NCVF = \frac{V_{NC}}{V_{patch}} \quad (5)$$

2.3. Myofiber Strain Calculations

The calculated strain $\epsilon(t)$ during the cardiac cycle represented the engineering strain based on the sarcomere length $L_s(t)$:

$$\epsilon(t) = \left(\frac{L_s(t)}{L_{s,ref}} - 1 \right) 100\% \quad (6)$$

where $L_{s,ref}$ is a reference sarcomere length used for strain calculations.

For the two-compartment model, the sarcomere length $L_s(t)$ of V_{patch} was calculated as the volume-weighted average of the

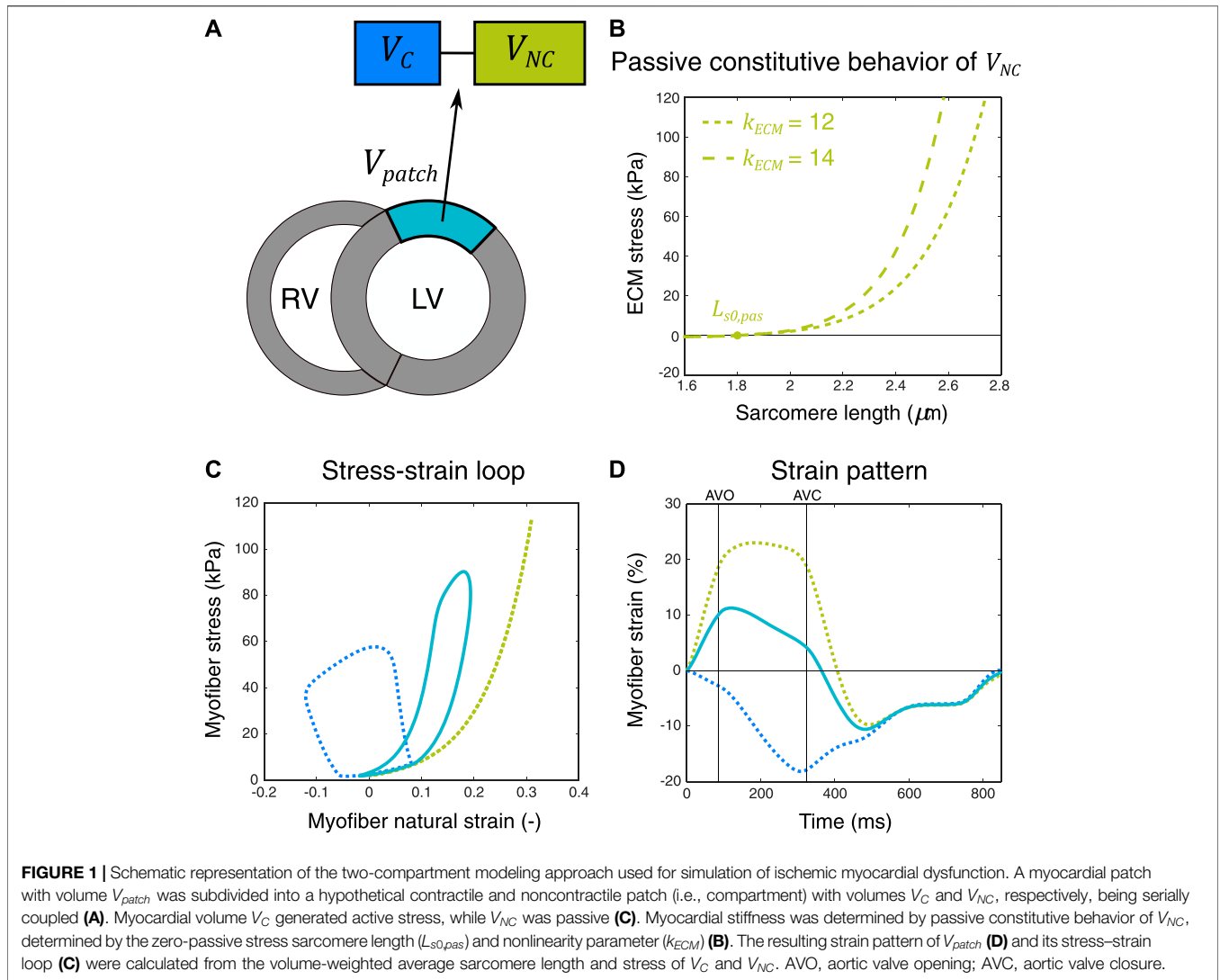


FIGURE 1 | Schematic representation of the two-compartment modeling approach used for simulation of ischemic myocardial dysfunction. A myocardial patch with volume V_{patch} was subdivided into a hypothetical contractile and noncontractile patch (i.e., compartment) with volumes V_C and V_{NC} , respectively, being serially coupled **(A)**. Myocardial volume V_C generated active stress, while V_{NC} was passive **(C)**. Myocardial stiffness was determined by passive constitutive behavior of V_{NC} , determined by the zero-passive stress sarcomere length ($L_{s0,pas}$) and nonlinearity parameter (k_{ECM}) **(B)**. The resulting strain pattern of V_{patch} **(D)** and its stress-strain loop **(C)** were calculated from the volume-weighted average sarcomere length and stress of V_C and V_{NC} . AVO, aortic valve opening; AVC, aortic valve closure.

sarcomere lengths of the contractile and noncontractile compartments, respectively, $L_{s,C}(t)$ and $L_{s,NC}(t)$:

$$L_s(t) = (1 - NCVF) \cdot L_{s,C}(t) + NCVF \cdot L_{s,NC}(t) \quad (7)$$

2.4 Simulation Protocol

2.4.1 Global Myocardial Mechanics:

One-Compartment Vs. Two-Compartment Model

In line with the study of Sunagawa et al. (1982), we compared simulated LV pump mechanics during acute regional ischemia when using a two-compartment model against a one-compartment model by constructing end-systolic pressure volume relations (ESPVRs). We started with a baseline reference simulation with a heart rate of 71 bpm, stroke volume (SV) of 72 ml, and a mean arterial pressure (MAP) of 92 mmHg. Homeostatic pressure-flow regulation was enabled, meaning that MAP and SV were kept constant through regulation of the peripheral arterial resistance and circulating blood volume. First, for the two-compartment simulation, the $NCVF$ was set to

0.2 in the LV free wall and septum to simulate 20% ischemia. Using the one-compartment model, $S_{f,act}$ in the LV and septal wall was gradually reduced until the LV end-diastolic volume was similar to that of the two-compartment simulation. Then, for both simulations of ischemia and for the baseline simulation, afterload manipulations were performed by increasing and reducing arterial resistance by 20% compared to the reference value, while disabling pressure-flow regulation, thereby constructing an ESPVR. The zero-pressure volume (V_0) and slope (E_{max}) of the ESPVR were calculated.

2.4.2 Regional Myocardial Mechanics: Acute Ischemia and Reperfusion

We hypothesized that acute ischemia and subsequent reperfusion could realistically be simulated by manipulation of the $NCVF$. To test this hypothesis, we used existing experimental data of regional myocardial deformation measured by sonomicrometry during acute 15-minute left anterior descending (LAD) coronary artery occlusion and subsequent reperfusion in a representative dog

(Figure 4A) (Lyseggen et al., 2005). The ultrasonic crystals used for sonomicrometry were implanted in the inner third of the myocardium of the anterior LV wall, which was aligned parallel with the LV long axis. We started with a baseline reference simulation with a similar heart rate (105 bpm) as in the experiment, and we modified MAP to obtain a similar LV peak systolic pressure (84 mmHg). The stroke volume was set to 49 ml to obtain a similar amplitude of segmental shortening as in the experiment. Starting from the baseline simulation, we simulated 15 min of LAD occlusion by increasing the *NCVF* from 0 to 1 in a myocardial region, which occupied 30% of the total LV wall volume and which was proportionally distributed over the septum and LV free wall. Assuming that the experimental ultrasonic crystals were placed entirely in the anterior LV wall, the strain and segment lengths in the model were calculated within the dysfunctional region located in the LV free wall. The sarcomere length L_s in the model was translated to the measured segment length SL by multiplying L_s with a constant, calculated from the difference between simulated end-diastolic L_s ($L_{s,ED}$) and the experimentally reported end-diastolic segment length ($SL_{exp,ED}$) in the baseline reference situation:

$$SL = L_s \cdot \frac{L_{s,ED}(\text{baseline})}{SL_{exp,ED}(\text{baseline})} \quad (8)$$

Parameters $L_{s0,pas}$ and k_{ECM} of V_{NC} (Eq. 3) were tuned to represent the experimental condition after 15 min of ischemia, that is, with similar end-diastolic segment length and systolic stretch amplitude. Starting from the simulation of 15-minute LAD occlusion, we reduced the *NCVF* from 1 to 0 with steps of 0.2 to simulate contractile recovery after reperfusion.

2.4.3 Regional Myocardial Mechanics: Prolonged Ischemia and Reperfusion

To evaluate whether the two-compartment model could also accurately simulate regional mechanics in ischemic dysfunction with increased stiffness, potentially indicating MI, we attempted to calibrate parameters $L_{s0,pas}$ and k_{ECM} to experimental data of regional myocardial deformation obtained after 4 h of the LAD occlusion followed by reperfusion (Lyseggen et al., 2005). We first calibrated the baseline reference simulation by setting the heart rate to the experimentally measured value of 111 bpm and tuning MAP such that the simulated peak LV systolic pressure was 91 mmHg. The stroke volume was set to 41 ml to obtain a similar amplitude of segmental shortening as in the experiment. Then, we again simulated acute anteroseptal ischemia occupying 30% of the total LV wall volume, with *NCVF* = 1 and values for $L_{s0,pas}$ and k_{ECM} tuned such that the end-diastolic segment length and systolic stretch amplitude were similar between the model and experiment. Starting from this simulation of acute ischemia, we modified k_{ECM} until the segmental systolic stretch in the model matched the reported stretch after 4 h of ischemia. We further modified k_{ECM} to obtain a similar systolic stretch as measured after 15 min of subsequent reperfusion. In both simulations, $L_{s0,pas}$ was tuned to obtain similar end-diastolic segment lengths between the model and experiment.

2.5 Patient-Specific *NCVF* Estimation

2.5.1 Patient Cohort

Six patients were selected from the DEFI-MI (DEtection of cardiac Fibrosis by LGE magnetic resonance imaging (MRI) and circulating biomarkers in patients with myocardial infarction) cohort. This was a prospective study on first-time MI patients, approved by the local ethics committee (METC: NL45241.041.13) and in accordance with the Declaration of Helsinki. Patients in this study were included after an acute MI, when urgent revascularization was performed. From the measured cohort, we selected patients with narrow QRS (<120 ms), who had a minimum infarct size of 10% of the LV wall mass and a minimum relative LGE percentage of 25% in at least one myocardial AHA segment.

2.5.2 Echocardiographic Measurements

Echocardiography was performed at the baseline (i.e., within 72 h after admission) and at the 6-month follow-up using a commercially available system (Vivid E9, GE Vingmed Ultrasound AS, Horten, Norway). LV volumes and ejection fraction (EF) were acquired by Simpson's biplane method. Focused loops of the apical four-chamber view, two-chamber view, and three-chamber view were stored for post-processing (GE EchoPAC version 203). Speckle tracking deformation imaging of the LV was performed in 18 segments according to current clinical standards while blinded to the MRI results (Voigt et al., 2015).

2.5.3 Cardiac Magnetic Resonance

At a median of 6 months after primary MI, all patients underwent contrast-enhanced 1.5 Tesla cardiac magnetic resonance (CMR) imaging (Philips Healthcare, Best, Netherlands). LGE image acquisition was performed 15 min after administration of 0.2 ml/kg gadobutrol (Gadovist, Bayer Vital GmbH, Leverkusen, Germany), using prospective ECG-gated sequences of the short axis views from the base to apex, with 5 mm slice thickness. Images were analyzed off-line using Philips ISP9 software (Philips Healthcare, Best, Netherlands). Using the RV insertion points to the interventricular septum as anatomical landmarks, the heart was subdivided into 16 segments according to the model of the American Heart Association (AHA) (Cerqueira et al., 2002), excluding the apical cap. The LGE was quantitatively assessed using the full width at half maximum (FWHM) method, providing a percentage for each of the analyzed segments and the total infarct (scar) size (global %) of the whole LV.

2.5.4 Optimization Algorithm

To estimate the *NCVF* on a segmental level, we used a multi-swarm particle swarm optimization (MSPSO) algorithm, as previously described by Van Osta et al. (2021). MSPSO is a stochastic optimization algorithm, which is highly suitable for nonlinear optimization problems. A brief description of the optimization algorithm will be provided here; for further methodological details, we referred to the study by Van Osta et al. (2021). As an input to the optimization algorithm, we used four different echocardiographic measurements (Figure 2,

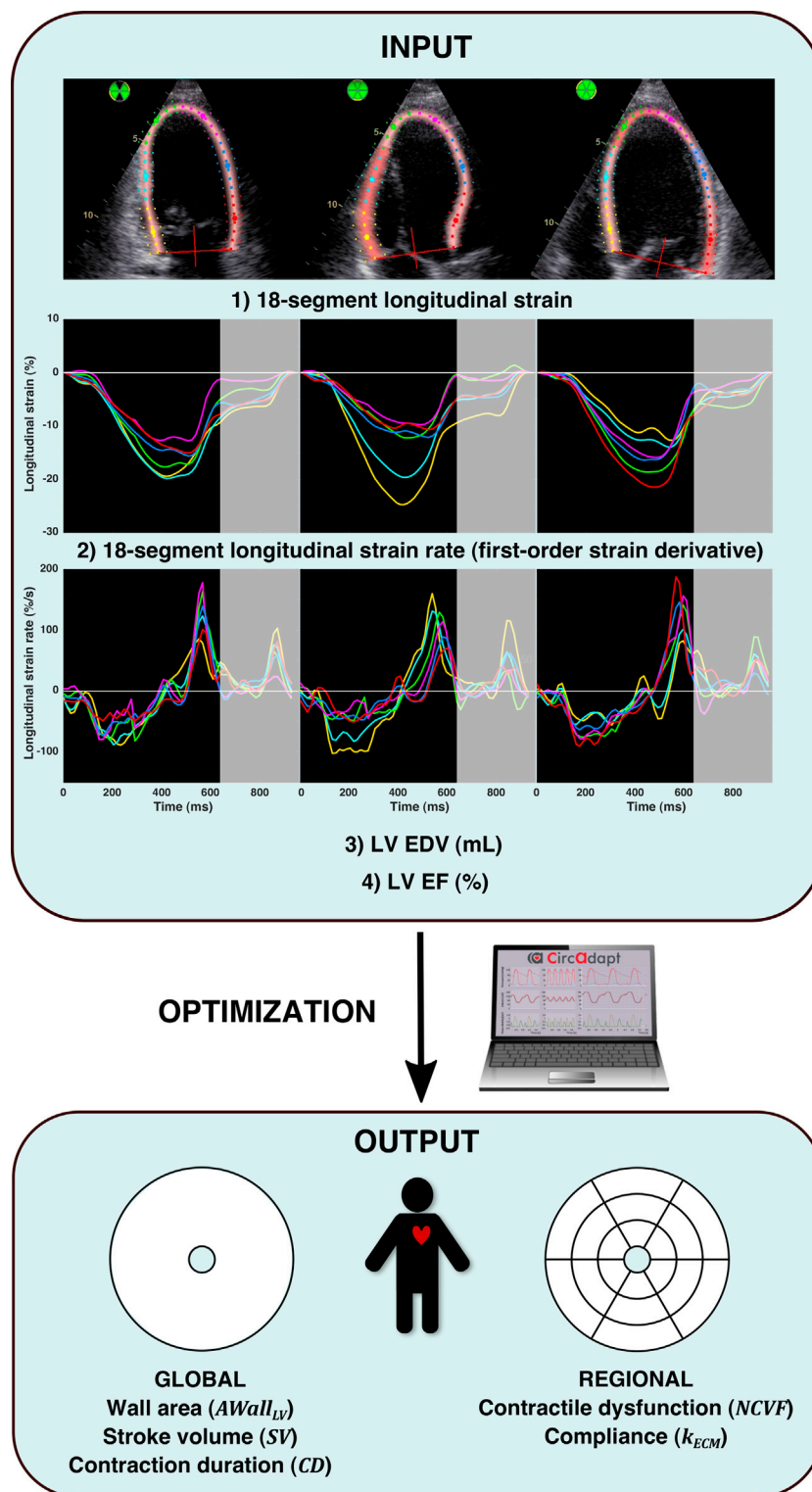


FIGURE 2 | Patient-specific parameter estimation protocol. The input of the optimization algorithm (INPUT) consisted of 1) 18-segment longitudinal strain, 2) 18-segment longitudinal strain rate (calculated as the first-order time derivative of strain), 3) LV end-diastolic volume (EDV), and 4) LV ejection fraction (EF). Strain and strain rate signals were analyzed until early diastole, as indicated by the gray-enhanced parts of the strain and strain rate signals. For numerical optimization (OPTIMIZATION), a multi-swarm particle swarm optimization (MSPSO) algorithm similar to the one previously described in the study by Van Osta et al. (2021) was run, which estimated (OUTPUT): global LV wall area, global stroke volume, global ventricular contraction duration, regional contractile dysfunction, and regional compliance.

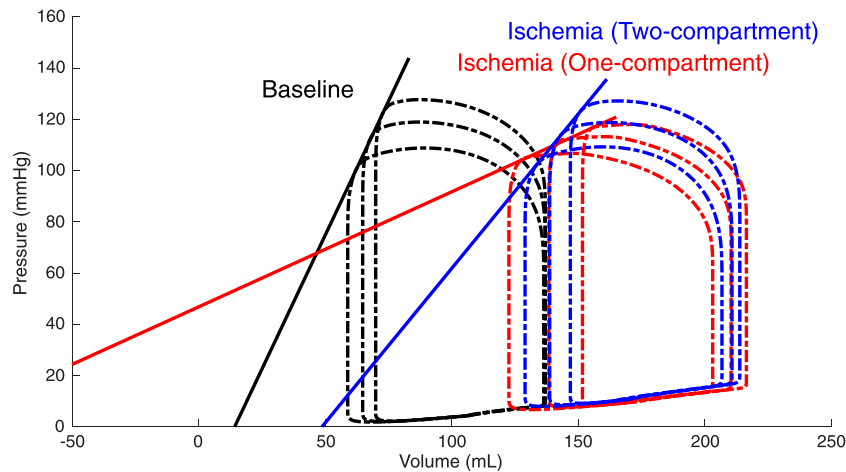


FIGURE 3 | Simulated left ventricular (LV) end-systolic pressure-volume relations (ESPVRs) for a baseline healthy LV (black loops and line) and for an ischemic LV affecting 20% of the LV wall mass modeled by a two-compartment approach (blue loops and line) and a one-compartment approach (red loops and line). ESPVRs were constructed by afterload manipulations through reducing and increasing arterial resistance by 20% compared to the reference resistance. The two-compartment simulation of ischemia demonstrated a rightward shift of the ESPVR with a moderate reduction in the slope, while the one-compartment simulation demonstrated a severe reduction in both the slope and zero-pressure volume.

TABLE 1 | Characteristics of the left ventricular (LV) end-systolic pressure–volume relation (ESPVR).

	V_0 (ml)	E_{max} (mmHg/ml)
Baseline	13.2	2.07
Ischemia (one-compartment)	-102.4	0.45
Ischemia (two-compartment)	46.7	1.21

INPUT): 1) the 18-segment longitudinal strain, 2) the 18-segment longitudinal strain rate, calculated as the first-order time-derivative of the strain signal, 3) the LV end-diastolic volume (EDV), and 4) the LV ejection fraction (EF). All four components were normalized in the objective function based on their expected measurement uncertainty, and simulated strains were also scaled to match the global strain amplitude between simulation and measurement. The strain and strain rate signals were analyzed until a pre-defined time point within the diastolic phase, defined as 10% of the cycle time after the moment of 10% global re-lengthening (i.e., global longitudinal strain (GLS) becomes less than 90% of its maximal value). The late diastolic strain was thereby neglected, considering the effects of, for example, drift compensation. Within the time interval analyzed, the sum of squared errors (SSEs) between the model and measurement was calculated, and the SSE was corrected for the number of time points. Parameters estimated in the model (Figure 2, OUTPUT) included the regional $NCVF$ and k_{ECM} , and global LV wall area $A_{wall,LV}$, global ventricular contraction duration CD , and stroke volume SV . Parameter estimation (Figure 2, OPTIMIZATION) was initiated by performing 1000 quasi-random Monte Carlo (MC) simulations with the heart rate (HR) set to the measured value. For each MC simulation, the objective function was calculated; in addition, for each individual segment, an error

was calculated as the sum of errors in the segmental strain and strain rate. A total of 40 initial candidate solutions were selected, which were the best 20 MC simulations based on the objective function and 20 random combinations of the best 20 segmental parameter sets (i.e., $NCVF$ and k_{ECM}) based on the segmental error. Subswarms were reassigned every 40 iterations, and MSPSO was stopped when either all particles had normalized energy $<10^{-4}$, meaning that within one iteration, all parameters changed by less than 1% of the width of their MC sampling domain, or a maximum number of 1000 iterations was reached.

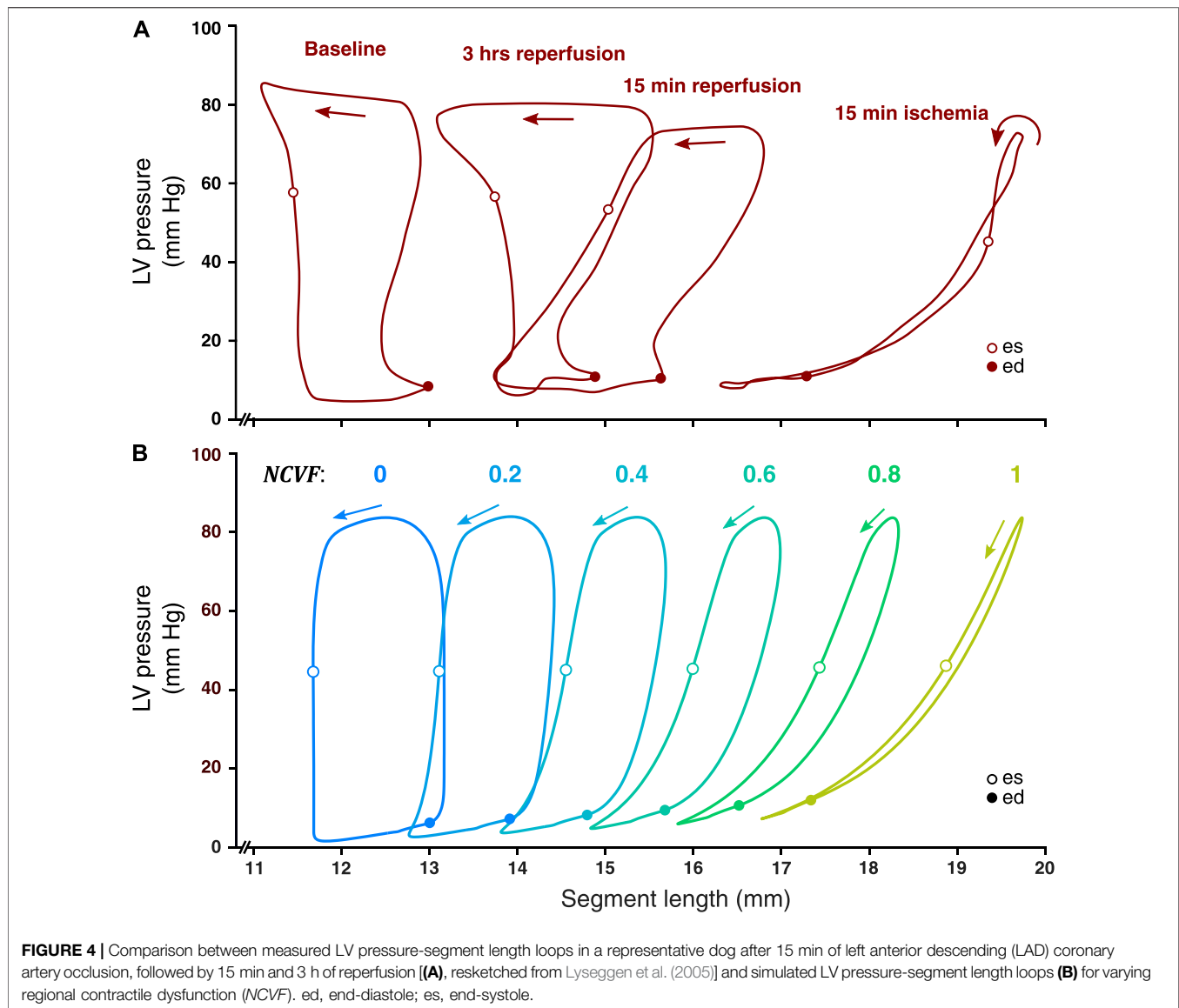
2.5.5 Model Implementation

The CircAdapt model used in this study has been published before in more detail (Walmsley et al., 2015). To reduce the computational cost, a C++ implementation of this version was used as published before (Van Osta et al., 2020). Equations were linearized using the Newton–Raphson method, and 61 ordinary differential equations were time-integrated using the Adams–Bashford method, with a variable timestep Δt with $\max(\Delta t) = 2$ ms. MSPSO was performed in MATLAB 2019a (MathWorks, Natick, MA, United States). Simulations ran in parallel on an AMD Ryzen Threadripper 3970X.

3 RESULTS

3.1 Global Myocardial Mechanics: One-Compartment Vs. Two-Compartment Model

Constructed ESPVRs for the one- and two-compartment simulations of LV acute regional ischemia are shown in Figure 3. The associated values of V_0 and E_{max} are provided in Table 1. Compared to the baseline simulation, E_{max} (2.07 mmHg/ml) was



moderately reduced for the two-compartment simulation (1.21 mmHg/ml), but it was severely reduced for the one-compartment simulation (0.45 mmHg/ml) of regional ischemia. Furthermore, with respect to the baseline V_0 (13.2 ml), V_0 was increased for the two-compartment simulation (46.7 ml), consistent with a rightward shift of the ESPVR, while the one-compartment simulation demonstrated a reduction of V_0 to -102.4 ml.

3.2 Regional Myocardial Mechanics: Acute Ischemia and Reperfusion

Simulated LV pressure-segment length loops and corresponding strain patterns at the baseline ($NCVF = 0$) and during acute ischemia ($NCVF = 1$) were successfully calibrated using the experimental measurements (Figures 4, 5). The calibrated parameter values are provided in Table 2, and an increase in

$L_{s0,pas}$ and k_{ECM} during acute ischemia with respect to the baseline is demonstrated. Starting from this simulation of acute ischemia, a reduction of the $NCVF$ shifted the LV pressure-segment length loop leftward, that is, back toward the baseline loop, while the loop area increased. The loops and strain patterns for $NCVF$ values of 0.4 and 0.2 were similar to the measured loops and strain patterns after 15 min and 3 h of reperfusion, respectively (Figures 4, 5).

3.3 Regional Myocardial Mechanics: Prolonged Ischemia and Reperfusion

When starting from the calibrated simulation of acute ischemia, increasing k_{ECM} led to a reduced amplitude of the segmental systolic stretch, while also shifting the LV pressure-segment length loop leftward (Figures 6, 7). Calibration of parameters $L_{s0,pas}$ and k_{ECM} demonstrated that a further

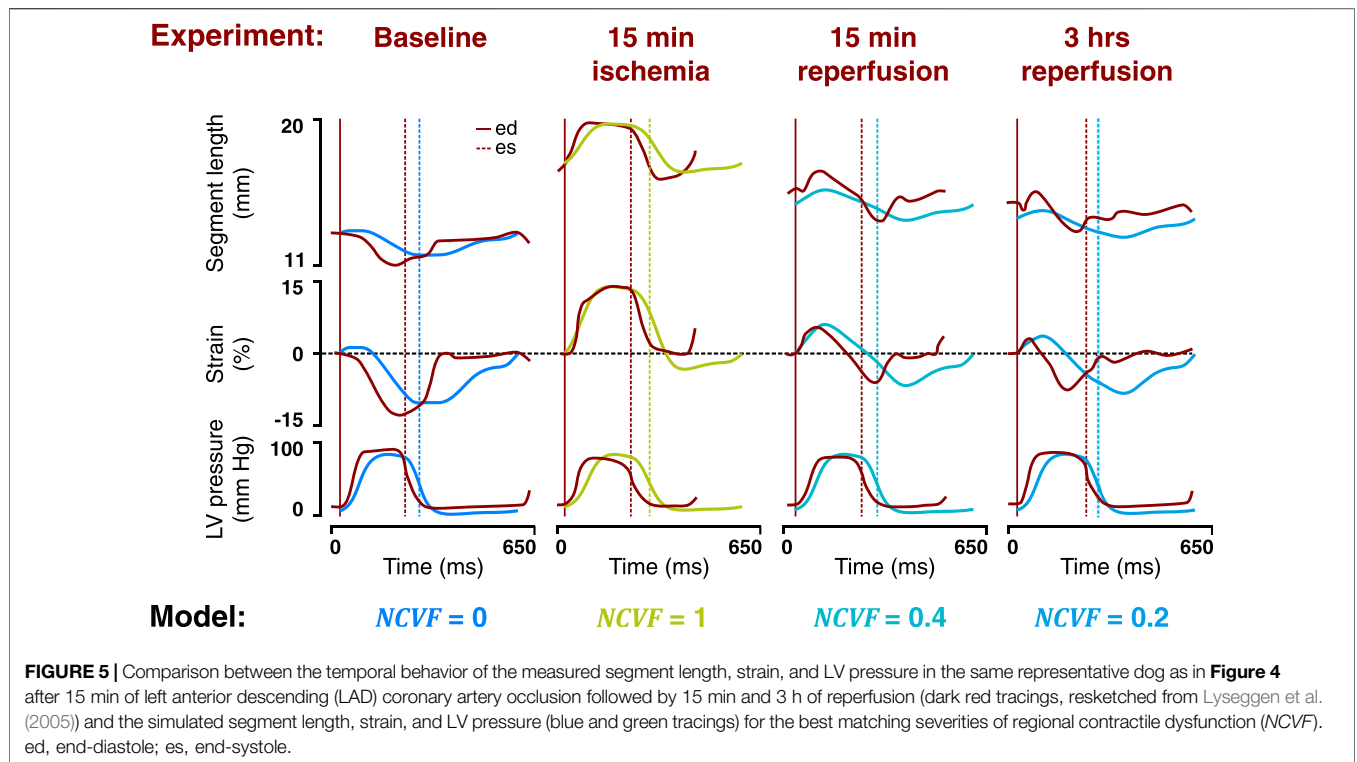


FIGURE 5 | Comparison between the temporal behavior of the measured segment length, strain, and LV pressure in the same representative dog as in **Figure 4** after 15 min of left anterior descending (LAD) coronary artery occlusion followed by 15 min and 3 h of reperfusion (dark red tracings, resketched from Lyseggen et al. (2005)) and the simulated segment length, strain, and LV pressure (blue and green tracings) for the best matching severities of regional contractile dysfunction (*NCVF*). ed, end-diastole; es, end-systole.

TABLE 2 | Calibrated parameter values for the simulations of acute ischemia and reperfusion.

	<i>NCVF</i> (-)	$L_{s0,pas}$ (μ m)	k_{ECM} (-)
Baseline	0	1.75 ^a	10 ^a
15-min ischemia	1	2.21	17
15-min reperfusion	0.4	2.21	17
3-h reperfusion	0.2	2.21	17

^aSince *NCVF* = 0, values of $L_{s0,pas}$ and k_{ECM} represent those of the contractile compartment V_C

increase of both $L_{s0,pas}$ and k_{ECM} was needed to reproduce the measured loop after 4 h of ischemia (**Table 3**), while a reduction of $L_{s0,pas}$ combined with a further increase of k_{ECM} was needed to reproduce the data after 15 min of subsequent reperfusion.

3.4 Patient-specific *NCVF* Estimation

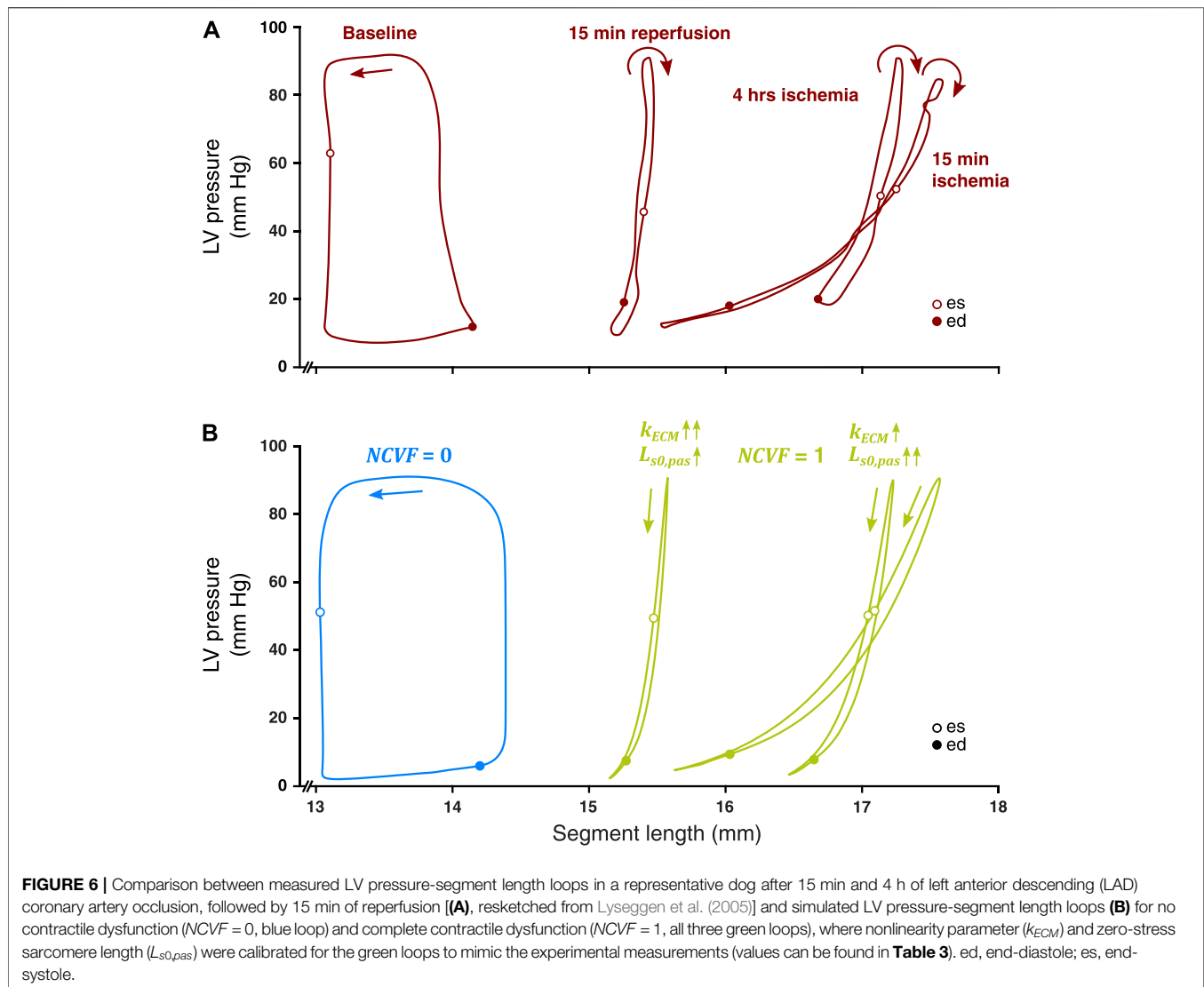
Patient characteristics are summarized in **Table 4**. Results of the patient-specific estimation of the *NCVF* for two different patients (patients 1 and 2) are shown in **Figures 8, 9**, respectively. For all four other patients, results are shown in **Supplementary Section S11.3**. In both patients 1 and 2, it can be noted that estimated *NCVF* values were increased in segments with increased systolic stretch or reduced peak systolic strain, both at the baseline and 6-month follow-up. In the acute phase after MI, patient 1 (**Figure 8**) demonstrated a localized area of increased *NCVF* in the anterior, anteroseptal, and inferoseptal segments, extending from the base all the way into the apex. At 6-month follow-up, LGE revealed the presence

of scar tissue within the same area, especially in the apical septal and mid-ventricular anterior and anteroseptal regions. While increased segmental *NCVF* values remained after 6 months, the *NCVF* in the anterior, anteroseptal, and inferoseptal segments were lower than at the baseline. This functional improvement over time was also reflected by an increase of LVEF from 30% at the baseline to 49% at 6-month follow-up. In patient 2 (**Figure 9**), increased values of *NCVF* at the baseline were found, especially in the apical anterior and septal segments, but it was extended into the mid-ventricular and basal segments. At 6-month follow-up, while the size of the region with increased *NCVF* was reduced, severe contractile dysfunction remained in the apex and mid-ventricular anteroseptal region. LGE revealed the presence of a large, transmural scar in this area.

Analysis of all 22 myocardial segments with LGE>25% at 6-month follow-up revealed that in most segments (68%), the *NCVF* was higher at the baseline than after 6 months (**Figure 10**). At the baseline, 21 (95%) segments had *NCVF* >25% and 12 (55%) had *NCVF* >50%, while at 6-month follow-up, 15 (68%) segments had *NCVF* >25% and 6 (27%) had *NCVF* >50%. Average segmental Δ *NCVF* between the baseline and 6-month follow-up was $-16.1 \pm 21.8\%$.

4 DISCUSSION

In this computational study, we used the CircAdapt model of the human heart and circulation to test the ability of a lumped two-compartment model to realistically simulate the effects of ischemia-induced contractile dysfunction on ventricular



pump and myocardial tissue mechanics. The modeling approach was first evaluated on the level of global LV mechanics by constructing ESPVRs at the baseline and during acute regional ischemia using simulations with a two- and one-compartment modeling approach. Then, simulated regional strains and pressure-length loops for increasing degrees of contractile dysfunction were compared with existing gold standard myocardial deformation measurements in dogs with acute and prolonged ischemia followed by reperfusion. Finally, patient-specific optimizations were performed to estimate the noncontractile volume fraction $NCVF$ in a small cohort of MI patients in the acute and chronic phase after MI, and estimated values were compared with LGE percentages after 6 months. Our results demonstrated that 1) global LV mechanics during regional ischemia were more realistically simulated by the two-compartment than the one-

compartment model, 2) manipulation of the $NCVF$ alone could reproduce the experimental deformation data on acute ischemia and subsequent reperfusion, while additional increases of myocardial stiffness were needed to reproduce the deformation data during prolonged ischemia followed by reperfusion, and 3) the patient-specific simulations further supported the idea that this modeling approach can potentially be used for strain-based estimation of regional myocardial contractile dysfunction in patients with cardiovascular disease.

4.1 Two-Compartment Model Realistically Simulates Global LV Mechanics

Constructed LV ESPVRs at baseline and during acute regional ischemia using both a one- and two-compartment modeling approach demonstrated that E_{max}

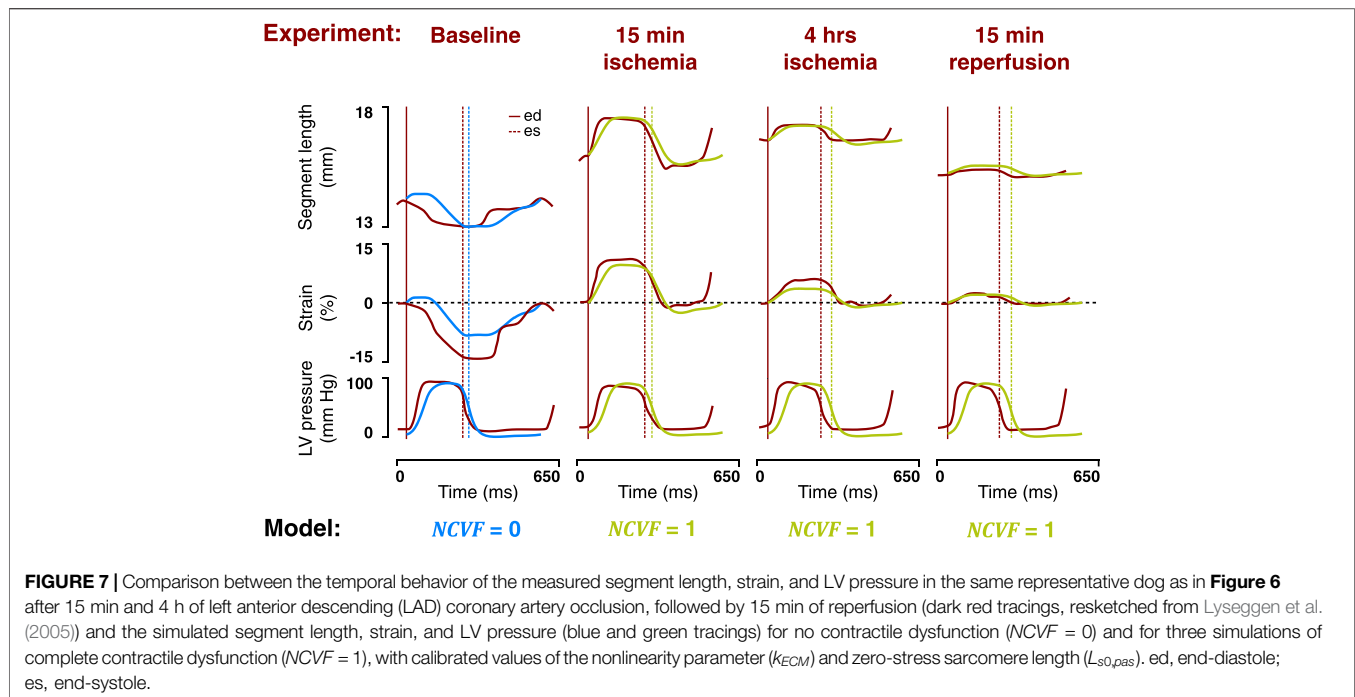


FIGURE 7 | Comparison between the temporal behavior of the measured segment length, strain, and LV pressure in the same representative dog as in **Figure 6** after 15 min and 4 h of left anterior descending (LAD) coronary artery occlusion, followed by 15 min of reperfusion (dark red tracings, resketched from Lyseggen et al. (2005)) and the simulated segment length, strain, and LV pressure (blue and green tracings) for no contractile dysfunction ($NCVF = 0$) and for three simulations of complete contractile dysfunction ($NCVF = 1$), with calibrated values of the nonlinearity parameter (k_{ECM}) and zero-stress sarcomere length ($L_{s0,pas}$). ed, end-diastole; es, end-systole.

TABLE 3 | Calibrated parameter values for the simulations of acute ischemia, prolonged ischemia, and reperfusion.

	NCVF (-)	$L_{s0,pas}$ (μm)	k_{ECM} (-)
Baseline	0	1.75 ^a	10 ^a
15-min ischemia	1	2.01	26
4-h ischemia	1	2.19	70
15-min reperfusion	1	2.03	120

^aSince $NCVF = 0$, values of $L_{s0,pas}$ and k_{ECM} represent those of the contractile compartment V_C

TABLE 4 | Patient characteristics of the selected DEFI-MI subcohort.

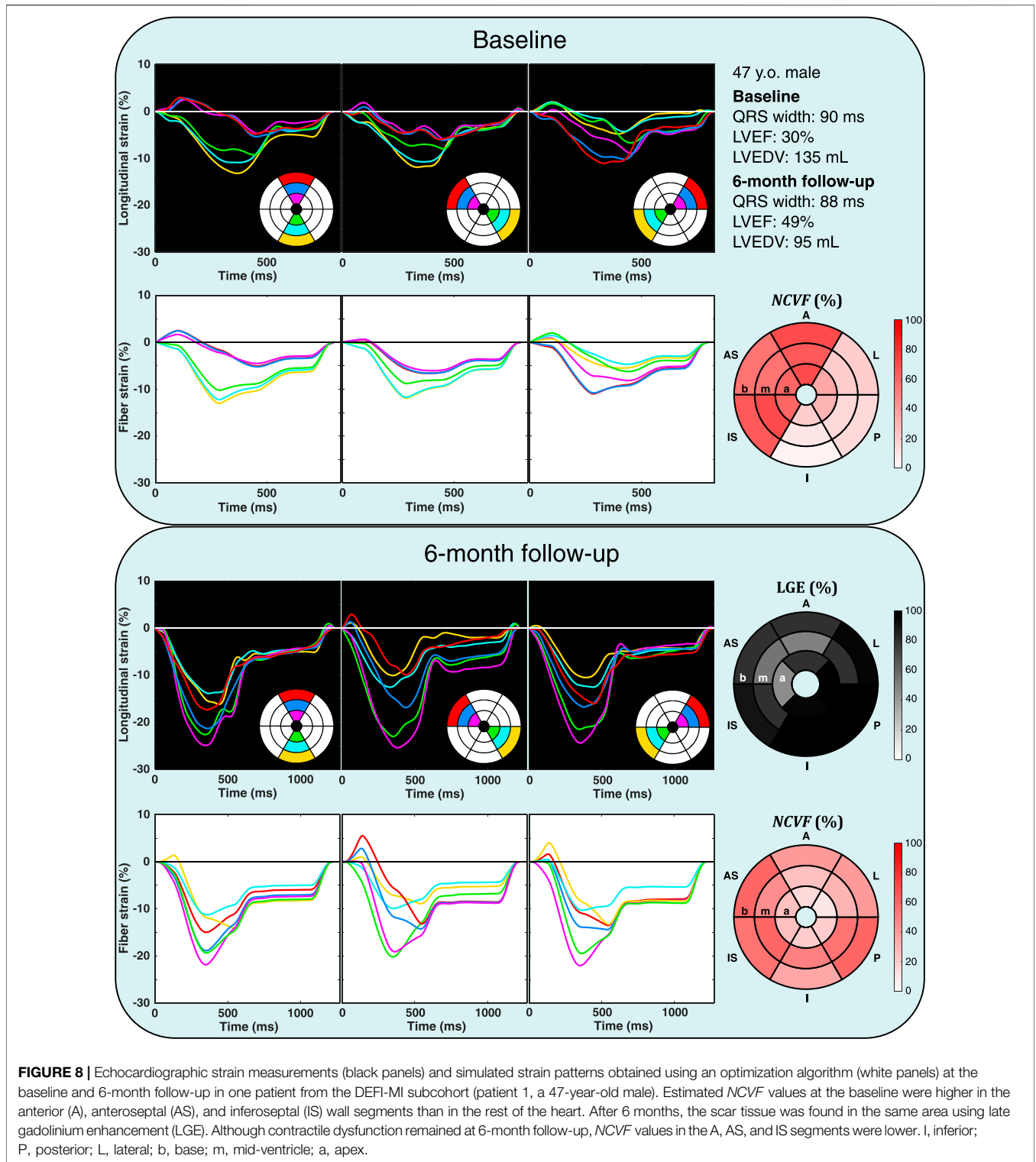
n	6 (83% Male)
Age at baseline (years)	57.6 ± 9.5
Relative infarct size (% of the LV wall mass)	16 ± 6
QRS duration baseline (ms)	90 ± 11
LVEF baseline (%)	49.8 ± 11.5
LVEDV baseline (ml)	100 ± 31
QRS duration 6-month follow-up (ms)	92 ± 13
LVEF 6-month follow-up (%)	50.5 ± 3.5
LVEDV 6-month follow-up (ml)	98 ± 25

was much less affected when a two-compartment model was used (**Figure 3; Table 1**). This result was expected and is in line with the observations of Sunagawa et al. (1982). In their study, they found no reduction in E_{max} for an ischemic region size of 20%; however, our simulation demonstrated a reduction of E_{max} from 2.07 mmHg/ml to 1.21 mmHg/ml.

This lower value of E_{max} in our simulation was likely caused by the relatively compliant passive tissue constitutive behavior, determined by the value of parameter k_{ECM} (**Eq. 3**). When increasing k_{ECM} , the nonlinearity of the passive stress-sarcomere length relation increases, which causes stiffer passive tissue behavior, thereby increasing E_{max} . This effect of infarct stiffness on the LV systolic function was also previously demonstrated in a modeling study by Fomovsky et al. (2011). It is noted that, at the same time, as a result of the parameterization of the passive tissue behavior, the change in V_0 with respect to the baseline (+33.5 ml) was more pronounced in our two-compartment model than in the experimental observations, where it was approximately +10 ml for an ischemic region size of 20% (Sunagawa et al., 1982). Qualitatively, however, a similar rightward shift of the ESPVR was observed. The one-compartment simulation of acute regional ischemia demonstrated a severe reduction of V_0 to a value of -102.4 ml, which is not consistent with experimental observations.

4.2 Two-Compartment Model Reproduces Regional Mechanics During Acute Ischemia and Reperfusion

Simulated strain patterns and LV pressure-segment length loops for $NCVF$ values of 1, 0.4, and 0.2 qualitatively agreed with the experimental data on acute ischemia followed by 15 min and 3 h of reperfusion, respectively (**Figures 4, 5**). While parameters $L_{s0,pas}$ and k_{ECM} were calibrated for the simulation of $NCVF = 1$ to match the reported end-diastolic segment length and systolic stretch amplitude during acute



ischemia, contractile recovery was simulated by reducing *NCVF* without further modifying $L_{s0,pas}$ and k_{ECM} (Table 2). This result supports *NCVF* as a parameter quantifying the degree of contractile dysfunction.

Calibrated parameter values for the simulation of acute ischemia demonstrated that $L_{s0,pas}$ and k_{ECM} were increased with respect to their baseline values. Increases in $L_{s0,pas}$ during acute ischemia have been reported in previous

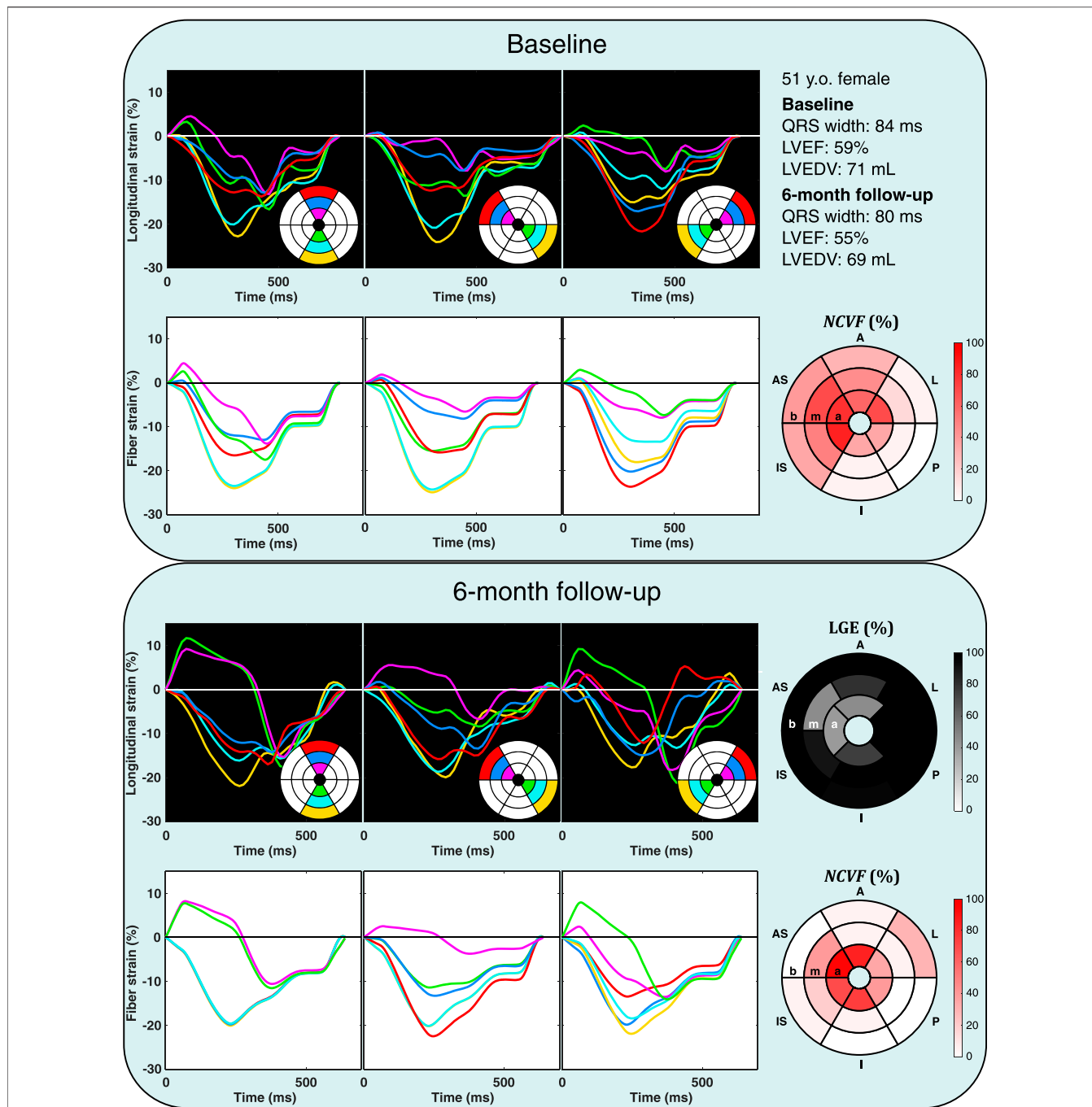
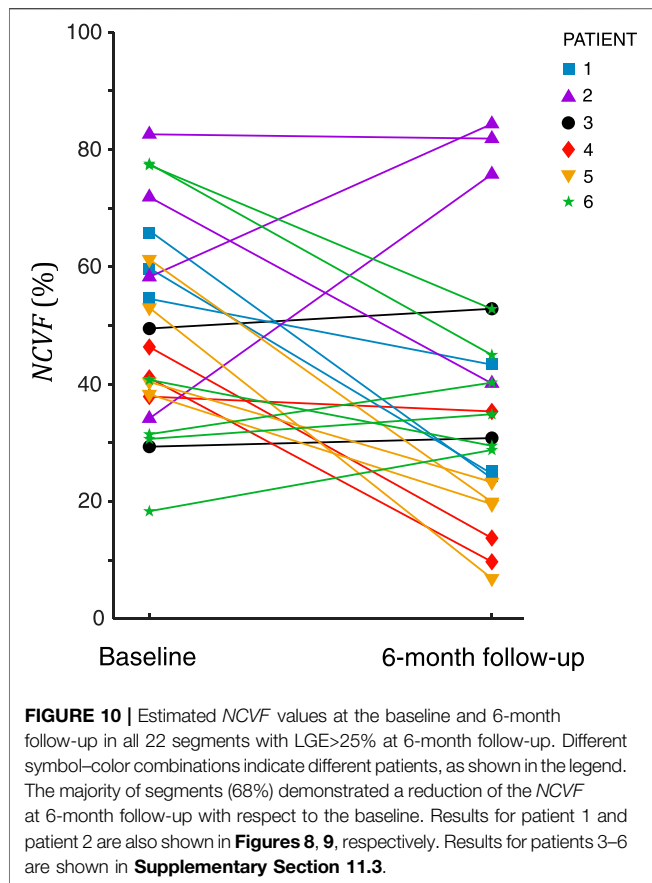


FIGURE 9 | Echocardiographic strain measurements (black panels) and simulated strain patterns obtained using an optimization algorithm (white panels) at the baseline and 6-month follow-up in one patient from the DEFI-MI subcohort (patient 2, a 51-year-old female). Estimated *NCVF* values at the baseline were higher in the anterior (A), anteroseptal (AS), and inferoseptal (IS) wall segments and in the apical (a) inferior (I), posterior (P), and lateral (L) wall segments than in the rest of the heart. After 6 months, the scar tissue was found using late gadolinium enhancement (LGE) in a part of this dysfunctional area, extending from the apex into the mid-ventricular (m) anteroseptal segment. Increased values of the *NCVF* were remained in these scarred segments. b, base.

studies, which have found that ischemic tissue dimensions were larger at matched pressures (Richardson et al., 2015). Adding to the discussion of the previous paragraph, the relatively large increase in k_{ECM} during acute ischemia

with respect to the baseline may indicate an inadequate parameterization of k_{ECM} in the baseline simulation, causing the myocardium to be too compliant. While immediate increases in tissue stiffness during acute



ischemia have been reported (Theroux et al., 1977), an acute effect of ischemia on tissue passive constitutive behavior has not clearly been established (Holmes et al., 2005). The data showed that after 3 h of reperfusion following acute ischemia, contractile recovery was still incomplete, which was confirmed by our simulations which demonstrated a good agreement with the data for $NCVF = 0.2$. This persistent dysfunction which follows reperfusion after a short-term period of ischemia has been attributed to myocardial stunning (Braunwald and Kloner, 1982). While it is known that stunning involves complex abnormalities at the cellular level including decreased calcium responsiveness (Gao et al., 1995), which are not explicitly described in our model, the parameter *NCVF* captured the mechanics during stunning relatively well.

4.3 Two-Compartment Model Reproduces Regional Mechanics During Prolonged Ischemia and Reperfusion

Our simulations of prolonged ischemia and subsequent reperfusion demonstrated that k_{ECM} was increased between 15 min and 4 h of ischemia and was even further increased after 15 min of subsequent reperfusion (**Figures 6, 7; Table 3**). This increased stiffness during prolonged ischemia, and reperfusion is in agreement with measurements of compliance performed in the experiment and

was linked to tissue edema as reflected by the increased myocardial water content (Lyseggen et al., 2005). The occurrence of interstitial edema and associated increases of myocardial stiffness during the necrotic phase have also been suggested in other studies (Holmes et al., 2005). At the same time, $L_{s0,pas}$ was increased between our simulations of 15 min and 4 h of ischemia, which may indicate early infarct expansion (Holmes et al., 2005). However, for the simulation of subsequent reperfusion, $L_{s0,pas}$ was again reduced, potentially indicating compaction of the necrotic region during the infarct healing process.

4.4 NCVF as a Measure of Ischemia-Induced Contractile Dysfunction

The parameter *NCVF* is defined in the model as the relative volume of the noncontractile compartment, and increasing *NCVF*, therefore, leads to increased contractile dysfunction. In the experimental dataset of acute ischemia and subsequent reperfusion, contractile recovery occurred, which was reflected by a reduction of *NCVF* in the model. However, in the dataset of prolonged ischemia and reperfusion, there was no contractile recovery, and contractile dysfunction remained at the same level ($NCVF = 1$). Similarly, the patient-specific *NCVF* estimations demonstrated that this parameter was increased in segments with systolic stretching or reduced peak systolic strain. Interestingly, in this patient cohort, among all segments with $LGE > 25\%$ 6 months after MI, *NCVF* values decreased substantially in most segments from the baseline to 6-month follow-up (**Figure 10**), suggesting partial recovery of myocardial contractile function over time. A possible explanation for this observed contractile recovery in the majority of segments is that most segments had nontransmural infarction at 6-month follow-up ($LGE < 50\%$), and nontransmural infarcts have been associated with functional recovery following revascularization (Ugander et al., 2010). Increased values of *NCVF* were found especially in segments with $LGE > 25\%$ after 6 months but were not limited to the *LGE*-positive segments. It is likely that nonscarred segments with increased *NCVF* in the acute phase after MI were dysfunctional due to myocardial stunning (Braunwald and Kloner, 1982). Increased *NCVF* values in nonscarred regions at 6-month follow-up could potentially be related to adverse myocardial remodeling. When we compared our obtained strain data and *NCVF* estimations with other modeling (Leong et al., 2017) and clinical studies (Zhang et al., 2005; Chan et al., 2006; Becker et al., 2009; Kihlberg et al., 2015; Huttin et al., 2016) of strain in MI, we noticed a common finding that transmural MI causes significant transmural strain abnormalities, including systolic stretching, a reduction of peak systolic strain, and post-systolic shortening. For subendocardial MI, Leong et al. (2017) found in their model that strain was affected in the subendocardial layers, but mid-myocardial and subepicardial strains were preserved. A similar conclusion was reached in a clinical study by Becker et al. (2009), who showed that nontransmural infarction led to greater functional impairment of the endocardial layer than of the epicardial layer. While this transmural heterogeneity in function may exist, multiple studies using strain or strain rate

imaging have successfully differentiated subendocardial MI from normal myocardium (Chan et al., 2006; Zhang et al., 2005) and thereby suggest that abnormal strains can be found in segments with subendocardial MI. The same suggestion holds for segments adjacent to an MI region, which have been shown to have a lower peak strain than segments remote from MI (McComb et al., 2015). From these and our own observations, we conclude that the *NCVF* is a functional parameter, which effectively indicates the degree of ischemia-induced contractile dysfunction; therefore, its use could enhance current diagnostics in patients with cardiovascular diseases. However, at the same time, *NCVF* alone seems to be unable to differentiate between underlying types of ischemic dysfunction; therefore, it is not suitable to replace LGE. Rather, it could provide useful diagnostic information on its own, or it could be used in addition to LGE.

4.5 Limitations

The experimental measurements of Lyseggen et al. (2005) used in our study were acquired by ultrasonic crystals which were aligned parallel to the LV long axis, thereby closely resembling the LV longitudinal strain. However, in our model, we used the one-fiber model to simulate the myofiber strain within a spherical LV geometry; therefore, there can be a systematic discrepancy between simulated and experimental strain values. In the patient-specific optimizations, we corrected for this model discrepancy by normalization of measured and simulated strains to global strain amplitude, but global strain values were not measured in the experiment; hence, no correction was performed. However, the temporal behavior of the experimental and simulated strains was similar; therefore, we expected that this potential mismatch could have had consequences for the quantitative values of calibrated parameters, but the qualitative results remained unaffected. We also assumed that the measurements were obtained from the anterior portion of the LV free wall, implying that we compared these data to simulated strains in the ischemic region located within the LV free wall, thereby disregarding septal deformation. This assumption, if not fully valid, could additionally have caused a minor mismatch in the strain data between the model and experiment. Furthermore, a sensitivity analysis (data not shown) demonstrated that correlations between the *NCVF* and passive material properties ($L_{s0,pas}$ and k_{ECM}) are very small or even absent and that *NCVF* is the parameter that most significantly determines the contractile function. Since $L_{s0,pas}$ and k_{ECM} are parameters which are modified in the noncontractile compartment only, they merely modify the end-diastolic sarcomere length and amplitude of systolic stretch, respectively, of the noncontractile compartment, thereby not impacting intrinsic myocardial contractility. Further research is needed to investigate whether and how $L_{s0,pas}$ and k_{ECM} are identifiable from regional strain measurements. The patient data used for this study were retrospectively obtained, and no arterial pressure measurements were available. We assumed that none of the patients had hypertension, and we set pressures in the model to default values. Since strain is known to depend on pre- and afterload (Skulstad et al., 2002; Ferferieva et al., 2012; P. Reant, 2016), this assumption on the patients' blood pressures could have influenced the strain signals. Furthermore, in our optimization protocol, the number of estimated parameters was limited. We did

not estimate, for example, the timing of mechanical activation, which potentially could also differ regionally in patients with MI due to slower electrical conduction in the scar tissue (Richardson et al., 2015). Further research is required to determine whether the set of estimated parameters was sufficient or could potentially be improved. In addition, we only used systolic and early diastolic strains for optimization in this study since we considered the late diastolic strain to be relatively inaccurate due to the effects of, for example, drift compensation. While we believe that the strain interval used is large enough for estimating the relevant parameters in this study, future studies could evaluate whether the late diastolic strain adds relevant information to the objective function.

5 CONCLUSION

We successfully used a two-compartment model for simulation of ventricular pump and myocardial tissue mechanics in ischemic heart disease. Patient-specific optimizations using regional myocardial deformation successfully estimated *NCVF* in a small cohort of MI patients in the acute and chronic phase after MI, while estimated *NCVF* values closely approximated the extent of myocardial scar at the follow-up. In future studies, this approach can facilitate deformation imaging-based estimation of myocardial tissue properties in patients with cardiovascular diseases.

DATA AVAILABILITY STATEMENT

The original contributions presented in the study are included in the article/**Supplementary Material**, further inquiries can be directed to the corresponding author.

ETHICS STATEMENT

The studies involving human participants were reviewed and approved by the METC: NL45241.041.13. The patients/participants provided their written informed consent to participate in this study.

AUTHOR CONTRIBUTIONS

TK and JL conceived the study. TK performed the simulations and wrote the first version of the manuscript. BK, FK and AT obtained the clinical data. NO, TL, FN, FP, BK, FK,AT, KV and TD helped with analysis and interpretation of the data. All co-authors critically read the manuscript and approved it.

FUNDING

This study was funded by the Dutch Heart Foundation (grant no. 2015T082 to JL), the Netherlands Organisation for Scientific

Research (grant 016.176.340), and the European Union's Horizon 2020 research and innovation programme under the Marie Skłodowska-Curie grant agreement no. 860745.

ACKNOWLEDGMENTS

The authors acknowledge the support from the Dutch Heart Foundation, the Netherlands Organisation for Scientific Research, and the European Union's Horizon 2020 research

and innovation programme under the Marie Skłodowska-Curie grant agreement.

SUPPLEMENTARY MATERIAL

The Supplementary Material for this article can be found online at: <https://www.frontiersin.org/articles/10.3389/fphys.2022.782592/full#supplementary-material>

REFERENCES

- Arts, T., Delhaas, T., Bovendeerd, P., Verbeek, X., and Prinzen, F. W. (2004). Adaptation to Mechanical Load Determines Shape and Properties of Heart and Circulation: the CircAdapt Model. *Am. J. Physiol. Heart Circ. Physiol.* 288 (4), H1943–H1954. doi:10.1152/ajpheart.00444.2004
- Arts, T., Bovendeerd, P., Delhaas, T., and Prinzen, F. (2003). Modeling the Relation between Cardiac Pump Function and Myofiber Mechanics. *J. Biomech.* 36 (5), 731–736. doi:10.1016/s0021-9290(02)00451-7
- Becker, M., Ocklenburg, C., Altiok, E., Futing, A., Balzer, J., Krombach, G., et al. (2009). Impact of Infarct Transmurality on Layer-specific Impairment of Myocardial Function: A Myocardial Deformation Imaging Study. *Eur. Heart J.* 30 (12), 1467–1476. doi:10.1093/eurheartj/ehp112
- Braunwald, E., and Kloner, R. A. (1982). The Stunned Myocardium: Prolonged, Postischemic Ventricular Dysfunction. *Circulation* 66 (6 I), 1146–1149. doi:10.1161/01.cir.66.6.1146
- Cerqueira, M. D., Weissman, N. J., Dilsizian, V., Jacobs, A. K., Kaul, S., Laskey, W. K., et al. (2002). Standardized Myocardial Segmentation and Nomenclature for Tomographic Imaging of the Heart. *J. Cardiovasc. Magn. Reson.* 4 (2), 203–210. doi:10.1081/jcmmr-120003946
- Chan, B. T., Ahmad Bakir, A., Al Abed, A., Dokos, S., Leong, C. N., Ooi, E. H., et al. (2019). Impact of Myocardial Infarction on Intraventricular Vortex and Flow Energetics Assessed Using Computational Simulations. *Int. J. Numer. Method. Biomed. Eng.* 35 (6), e3204–17. doi:10.1002/cnm.3204
- Chan, J., Hanekom, L., Wong, C., Leano, R., Cho, G.-Y., and Marwick, T. H. (2006). Differentiation of Subendocardial and Transmural Infarction Using Two-Dimensional Strain Rate Imaging to Assess Short-Axis and Long-Axis Myocardial Function. *J. Am. Coll. Cardiol.* 48 (10), 2026–2033. doi:10.1016/j.jacc.2006.07.050
- Estrada, A. C., Yoshida, K., Clarke, S. A., and Holmes, J. W. (2020). Longitudinal Reinforcement of Acute Myocardial Infarcts Improves Function by Transmurally Redistributing Stretch and Stress. *J. Biomech. Eng.* 142 (2), 1–10. doi:10.1115/1.4044030
- Fan, Y., Ronan, W., Teh, I., Schneider, J. E., Varela, C. E., Whyte, W., et al. (2019). A Comparison of Two Quasi-Static Computational Models for Assessment of Intra-myocardial Injection as a Therapeutic Strategy for Heart Failure. *Int. J. Numer. Method. Biomed. Eng.* 35 (9), e3213. doi:10.1002/cnm.3213
- Ferferieva, V., Van den Bergh, A., Claus, P., Jasaityte, R., Veulemans, P., Pellens, M., et al. (2012). The Relative Value of Strain and Strain Rate for Defining Intrinsic Myocardial Function. *Am. J. Physiol. Heart Circ. Physiol.* 302 (1), H188–H195. doi:10.1152/ajpheart.00429.2011
- Fomovsky, G. M., MacAdangdang, J. R., Ailawadi, G., and Holmes, J. W. (2011). Model-based Design of Mechanical Therapies for Myocardial Infarction. *J. Cardiovasc. Trans. Res.* 4 (1), 82–91. doi:10.1007/s12265-010-9241-3
- Fomovsky, G. M., Rouillard, A. D., and Holmes, J. W. (2012). Regional Mechanics Determine Collagen Fiber Structure in Healing Myocardial Infarcts. *J. Mol. Cell Cardiol.* 52 (5), 1083–1090. doi:10.1016/j.yjmcc.2012.02.012
- Gao, W. D., Atar, D., Backx, P. H., and Marban, E. (1995). Relationship between Intracellular Calcium and Contractile Force in Stunned Myocardium. *Circ. Res.* 76 (6), 1036–1048. doi:10.1161/01.res.76.6.1036
- Haddad, S. M. H., and Samani, A. (2018). A Finite Element Model of Myocardial Infarction Using a Composite Material Approach. *Comput. Methods Biomed. Biomed. Eng.* 21 (1), 33–46. doi:10.1080/10255842.2017.1416355
- Holmes, J. W., and Lumens, J. (2018). Clinical Applications of Patient-specific Models: The Case for a Simple Approach. *J. Cardiovasc. Transl. Res.* 11 (1–9), 71–79. doi:10.1007/s12265-018-9787-z
- Holmes, J. W., Borg, T. K., and Covell, J. W. (2005). Structure and Mechanics of Healing Myocardial Infarcts. *Annu. Rev. Biomed. Eng.* 7 (1), 223–253. doi:10.1146/annurev.bioeng.7.060804.100453
- Huttin, O., Marie, P.-Y., Benichou, M., Bozec, E., Lemoine, S., Mandry, D., et al. (2016). Temporal Deformation Pattern in Acute and Late Phases of ST-Elevation Myocardial Infarction: Incremental Value of Longitudinal post-systolic Strain to Assess Myocardial Viability. *Clin. Res. Cardiol.* 105 (10), 815–826. doi:10.1007/s00392-016-0989-6
- Kihlberg, J., Haraldsson, H., Sigfridsson, A., Ebberts, T., and Engvall, J. E. (2015). Clinical Experience of Strain Imaging Using DENSE for Detecting Infarcted Cardiac Segments. *J. Cardiovasc. Magn. Reson.* 17 (1), 50–59. doi:10.1186/s12968-015-0155-8
- Leong, C. N., Lim, E., Andriyana, A., Al Abed, A., Lovell, N. H., Hayward, C., et al. (2017). The Role of Infarct Transmural Extent in Infarct Extension: A Computational Study. *Int. J. Numer. Method. Biomed. Eng.* 33 (2), 1–18. doi:10.1002/cnm.2794
- Lumens, J., Tayal, B., Walmsley, J., Delgado-Montero, A., Huntjens, P. R., Schwartzman, D., et al. (2015). Differentiating Electromechanical from Non-electrical Substrates of Mechanical Discoordination to Identify Responders to Cardiac Resynchronization Therapy. *Circ. Cardiovasc. Imaging* 8 (9), e003744–12. doi:10.1161/CIRCIMAGING.115.003744
- Lumens, J., Delhaas, T., Kirn, B., and Arts, T. (2009). Three-wall Segment (TriSeg) Model Describing Mechanics and Hemodynamics of Ventricular Interaction. *Ann. Biomed. Eng.* 37 (11), 2234–2255. doi:10.1007/s10439-009-9774-2
- Lyseggen, E., Skulstad, H., Helle-Valle, T., Vartdal, T., Urheim, S., Rabben, S. I., et al. (2005). Myocardial Strain Analysis in Acute Coronary Occlusion. *Circulation* 112 (25), 3901–3910. doi:10.1161/circulationaha.105.533372
- McComb, C., Carrick, D., McClure, J. D., Woodward, R., Radjenovic, A., Foster, J. E., et al. (2015). Assessment of the Relationships between Myocardial Contractility and Infarct Tissue Revealed by Serial Magnetic Resonance Imaging in Patients with Acute Myocardial Infarction. *Int. J. Cardiovasc. Imaging* 31 (6), 1201–1209. doi:10.1007/s10554-015-0678-y
- Moulton, M. J., Hong, B. D., and Secomb, T. W. (2017). Simulation of Left Ventricular Dynamics Using a Low-Order Mathematical Model. *Cardiovasc. Eng. Tech.* 8 (4), 480–494. doi:10.1007/s13239-017-0327-9
- P. Reant (2016). Impact of Afterload Increase on Left Ventricular Myocardial Deformation Indices. *J. Am. Soc. Echocardiogr.* 29, 1217–1228. doi:10.1016/j.echo.2016.09.006
- Richardson, W. J., Clarke, S. A., Quinn, T. A., and Holmes, J. W. (2015). Physiological Implications of Myocardial Scar Structure. *Compr. Physiol.* 5 (4), 1877–1909. doi:10.1002/cphy.c140067
- Rouillard, A. D., and Holmes, J. W. (2014). Coupled Agent-Based and Finite-Element Models for Predicting Scar Structure Following Myocardial Infarction. *Prog. Biophys. Mol. Biol.* 115 (2–3), 235–243. doi:10.1016/j.pbiomolbio.2014.06.010
- Skulstad, H., Edvardsen, T., Urheim, S., Rabben, S. I., Stugaard, M., Lyseggen, E., et al. (2002). Postsystolic Shortening in Ischemic Myocardium. *Circulation* 106 (6), 718–724. doi:10.1161/01.cir.0000024102.55150.b6
- Sunagawa, K., Maughan, W. L., and Sagawa, K. (1982). *Effect of Regional Ischemia on the Left Ventricular End-Systolic Pressure-Volume Relationship of Isolated Canine Hearts*, 170–179.

- Theroux, P., Ross, J., Franklin, D., Covell, J. W., Bloor, C. M., and Sasayama, S. (1977). Regional Myocardial Function and Dimensions Early and Late after Myocardial Infarction in the Unanesthetized Dog. *Circ. Res.* 40 (2), 158–165. doi:10.1161/01.res.40.2.158
- Ugander, M., Cain, P. A., Johnsson, P., Palmer, J., and Arheden, H. (2010). Chronic Non-transmural Infarction Has a Delayed Recovery of Function Following Revascularization. *BMC Cardiovasc. Disord.* 10, 4. doi:10.1186/1471-2261-10-4
- Van Osta, N., Kirkels, F., Lyon, A., Koopsen, T., van Loon, T., Cramer, M. J., et al. (2021). Electromechanical Substrate Characterization in Arrhythmogenic Cardiomyopathy Using Imaging-Based Patient-specific Computer Simulations. *Europace* 23, I153–I160. doi:10.1093/europace/eaab407
- Van Osta, N., Lyon, A., Kirkels, F., Koopsen, T., van Loon, T., Cramer, M. J., et al. (2020). Parameter Subset Reduction for Patient-specific Modelling of Arrhythmogenic Cardiomyopathy-Related Mutation Carriers in the CircAdapt Model. *Philos. Trans. A. Math. Phys. Eng. Sci.* 378, 20190347. doi:10.1098/rsta.2019.0347
- Veress, A. I., Fung, G. S., Lee, T. S., Tsui, B. M., Kicska, G. A., Paul Segars, W., et al. (2015). The Direct Incorporation of Perfusion Defect Information to Define Ischemia and Infarction in a Finite Element Model of the Left Ventricle. *J. Biomech. Eng.* 137 (5), 051004–051010. doi:10.1115/1.4028989
- Voigt, J.-U., Pedrizzetti, G., Lysyansky, P., Marwick, T. H., Houle, H., Baumann, R., et al. (2015). Definitions for a Common Standard for 2D Speckle Tracking Echocardiography: Consensus Document of the EACVI/ASE/Industry Task Force to Standardize Deformation Imaging. *Eur. Heart J. - Cardiovasc. Imaging* 16 (1), 1–11. doi:10.1093/ehjci/jeu184
- Walmsley, J., Arts, T., Derval, N., Bordachar, P., Cochet, H., Ploux, S., et al. (2015). Fast Simulation of Mechanical Heterogeneity in the Electrically Asynchronous Heart Using the MultiPatch Module. *Plos Comput. Biol.* 11 (7), e1004284–23. doi:10.1371/journal.pcbi.1004284
- Wang, H., Rodell, C. B., Zhang, X., Dusaj, N. N., Gorman, J. H., Pilla, J. J., et al. (2018). Effects of Hydrogel Injection on Borderzone Contractility post-myocardial Infarction. *Biomech. Model. Mechanobiol.* 17 (5), 1533–1542. doi:10.1007/s10237-018-1039-2
- Zhang, Y., Wang, V. Y., Morgan, A. E., Kim, J., Ge, L., Guccione, J. M., et al. (2020). A Novel MRI-Based Finite Element Modeling Method for Calculation of Myocardial Ischemia Effect in Patients with Functional Mitral Regurgitation. *Front. Physiol.* 11, 158. doi:10.3389/fphys.2020.00158
- Zhang, Y., Chan, A. K. Y., Yu, C.-M., Yip, G. W. K., Fung, J. W. H., Lam, W. W. M., et al. (2005). Strain Rate Imaging Differentiates Transmural from Non-transmural Myocardial Infarction. *J. Am. Coll. Cardiol.* 46 (5), 864–871. doi:10.1016/j.jacc.2005.05.054
- Zhang, Y., Wang, V. Y., Morgan, A. E., Kim, J., Tafreshi, R., Wallace, A. W., et al. (2021). Finite-element Based Optimization of Left Ventricular Passive Stiffness in normal Volunteers and Patients after Myocardial Infarction: Utility of an Inverse Deformation Gradient Calculation of Regional Diastolic Strain. *J. Mech. Behav. Biomed. Mater.* 119, 104431. doi:10.1016/j.jmbbm.2021.104431
- Zhuan, X., Luo, X., Gao, H., and Ogden, R. W. (2019). Coupled Agent-Based and Hyperelastic Modelling of the Left Ventricle post-myocardial Infarction. *Int. J. Numer. Method. Biomed. Eng.* 35 (1), e3155–18. doi:10.1002/cnm.3155

Conflict of Interest: The authors declare that the research was conducted in the absence of any commercial or financial relationships that could be construed as a potential conflict of interest.

Publisher's Note: All claims expressed in this article are solely those of the authors and do not necessarily represent those of their affiliated organizations, or those of the publisher, the editors, and the reviewers. Any product that may be evaluated in this article, or claim that may be made by its manufacturer, is not guaranteed or endorsed by the publisher.

Copyright © 2022 Koopsen, Van Osta, Van Loon, Van Nieuwenhoven, Prinzen, Van Klarenbosch, Kirkels, Teske, Vernooy, Delhaas and Lumens. This is an open-access article distributed under the terms of the Creative Commons Attribution License (CC BY). The use, distribution or reproduction in other forums is permitted, provided the original author(s) and the copyright owner(s) are credited and that the original publication in this journal is cited, in accordance with accepted academic practice. No use, distribution or reproduction is permitted which does not comply with these terms.